Journal of Materials Chemistry A

Accepted Manuscript

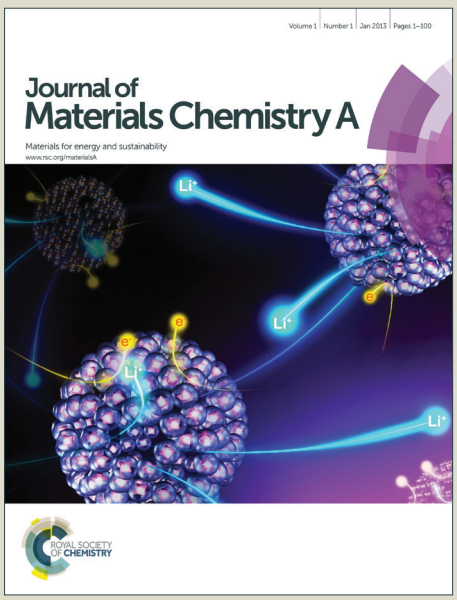

ROYAL SOCIETY OF CHEMISTRY

www.rsc.org/materialsA

Graphical Abstract

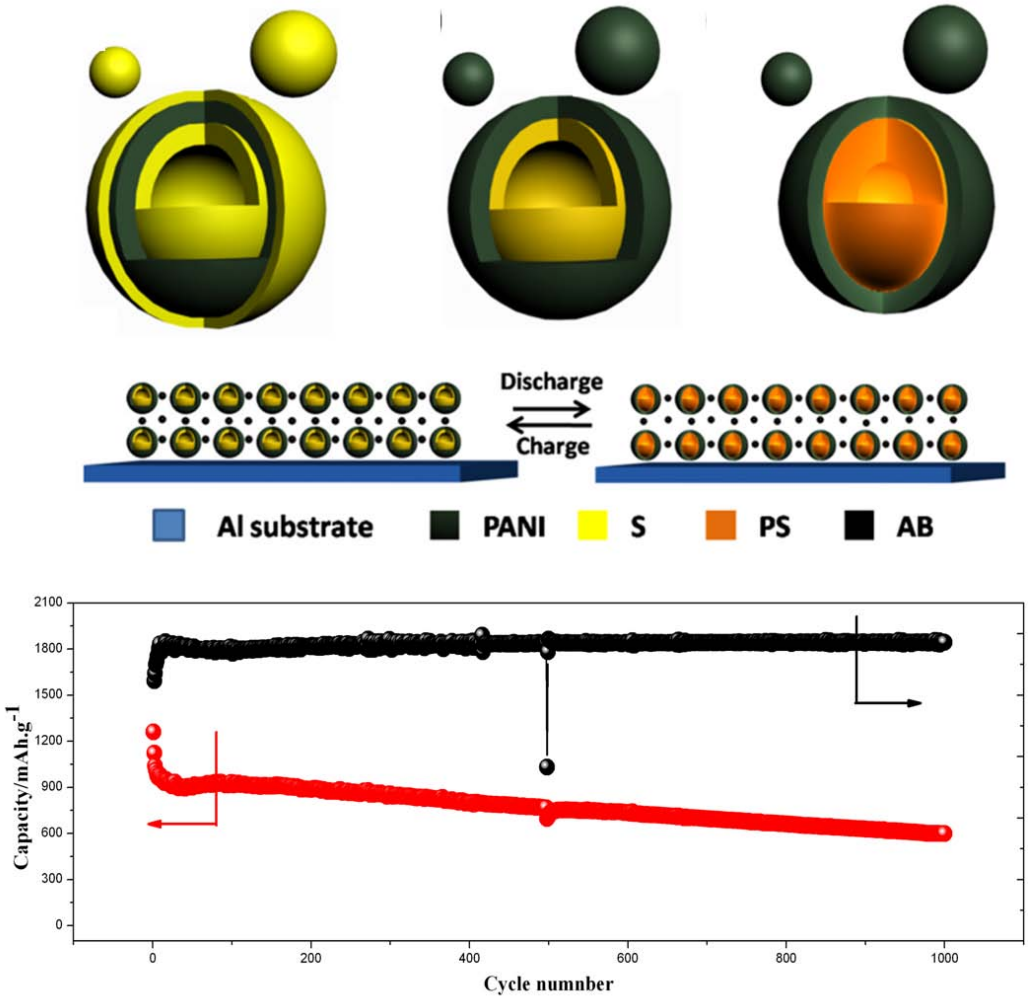

Cite this: DOI: 10.1039/c0xx00000x

www.rsc.org/xxxxxx

ARTICLE TYPE

Hollow Polyaniline sphere@Sulfur Composites for Prolonged cycling Stability of Lithium Sulfur batteries

Guoqiang Ma[a], Zhaoyin Wen*[a], Jun Jin[a], Yan Lu[a], Xiangwei Wu[a], Meifen Wu[a] and Chunhua Chen[b]

Received (in XXX, XXX) Xth XXXXXXXXX 20XX, Accepted Xth XXXXXXXXX 20XX

DOI: 10.1039/b000000x

A sulfur cathode with excellent electrochemical performance has been designed based on hollow PANI spheres, which can suppress shuttle effect and buffer the volume expansion effectively. The discharge capacity is as high as 602mAh.g^{-1} even after 1000 cycles at 0.5C.

Rechargeable batteries with high specific energy are essential for solving imminent energy and environmental issues[1-6]. Li-ion batteries have one of the highest specific energies among rechargeable batteries. Those based on intercalation mechanism has a theoretical specific energy of ~400Wh.Kg^{-1} for both $LiCoO_2$/graphite and $LiFePO_4$/ graphite systems[7]. To achieve higher specific energy, new materials for both cathode and anode are required. Among various types of cathode materials, sulfur cathode has attracted increasing attention due to its high theoretical specific capacity (1675mAh.g^{-1}) and energy density (2600Wh.Kg^{-1}). These are several times greater than those of common lithium-ion batteries. In combination with the natural abundance, low cost and environmental friendliness of sulfur, the Li-S battery becomes a promising candidate for the next generation power source[2, 3, 5, 8-10].

The low utilization of active-sulfur material, poor cycling performance and low coulombic efficiency of Li-S batteries have become significant hindrance toward their commercialization[11, 12]. The low utilization rate of sulfur is due to the high insulating nature of sulfur (σ=5×10^{-30} S.cm^{-1} at 25℃). The fast capacity fading during cycling and the poor rate stability can be attributed to a variety of factors, including a high solubility of lithium polysulfides (PS) (Li_2S_x, $2<x\leq8$) in the electrolyte and the large volume expansion rate (80%) for sulfur during the charge/discharge process[13]. The PS dissolved in the electrolyte could diffuse to the lithium anode, resulting in undesired corrosion reaction, and the loss of active material. Furthermore, once discharge is initiated, a redistribution of PS on the electrode results in the deposition and aggregation of sulfur on the surface of cathode. This limits the complete penetration of the electrolyte into the whole electrode, which also accounts for the rapid capacity fading[14]. As a result, the combination of enhancement the of ionic and electronic conductivity of the cathode, efficient trapping of PS and suppression of the volume expansion is highly desired for improving the cycle life of Li-S batteries[3, 12, 15].

Various approaches have been attempted to achieve these aims, including the optimization of the organic electrolyte[16-21], the preparation of sulfur/carbon composites[22-30], the fabrication of sulfur/polymer composite[31-37], and the employment of Li_2S as the active material of the cathode[38-41]. Furthermore, the modification of separator[42, 43] , the current collector[44-46] and the protection of lithium anode[47, 48] are also effective strategies to improve the electrochemical performance of Li-S batteries.

A core-shell structure, which can improve the conductivity of the cathode and suppress the dissolution of polysulfide simultaneously, has been considered as the effective approach to enhance the electrochemical performance of Li-S battery. Archer and coworkers synthesized mesoporous hollow carbon sphere-sulfur composite, which displays a reversible capacity of about 850mAh.g^{-1} after 100 cycles at a discharge rate of 0.5C[24]. Cui's group developed a sulfur-TiO_2 yolk-shell microstructure. The capacity decay after 1,000 cycles is as small as 0.033% per cycle with an average coulombic efficiency of 98% at 0.5C, This is considered as an exciting result for Li-S battery[13, 49]. Simultaneously, Cui's group also reported a nano-structural polymer-wrapped hollow sulfur nano-spheres based composite with enhanced specific capacity and cycling performance[50].

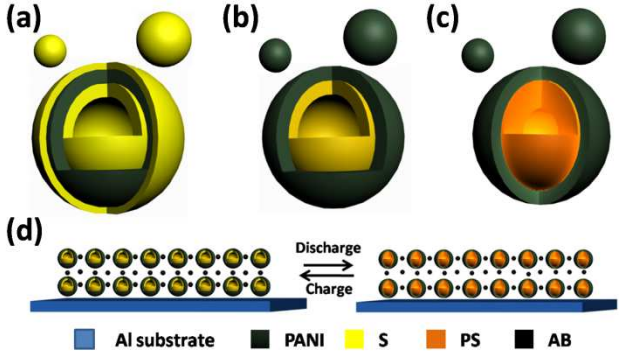

Fig.1 The schematics of PANI-S composite during charge/discharge process, (a) the original PANI-S composite, (b) the cycled PANI-S composite, (c) the lithiated PANI-S composite, (d) Schematic illustration of integrity of the hollow PANI-S electrode with serious expansion and shrinkage during discharge and charge processes.

PANI is attractive among the family of conductive polymers because of its associated electrical, electrochemical, and optical properties, free volume, coupled with excellent environmental stability[51-53]. Here, we report a conductive polymer (PANI) hollow sphere, which is fabricated and used as the matrix of sulfur by vapour phase infusion method. Referring to Fig.1 (a), with vapour phase infusion method, sulfur is attached on both the inner and outer surface of PANI hollow spheres. Sulfur coating on the outer-surface of PANI hollow spheres will be dissolved during the first several cycles (Fig.1b), but the dissolution of the sulfur in the hollow PANI sphere will be suppressed effectively, and the volume expansion during the charge/discharge is buffered by the void space in the PANI-S nano-particles (Fig.1c, Fig.1d). Furthermore, the chemical bond generated during heating treatment process between PANI and S is beneficial for suppressing shuttle effect[31, 54, 55]. Therefore, it is predictable for the PANI-S cathode to get an excellent electrochemical performance.

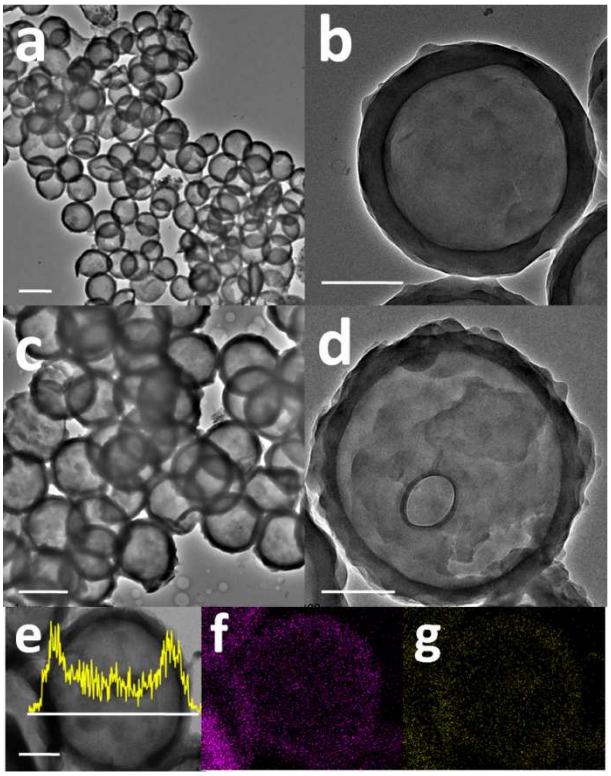

Fig.2 TEM images of PANI hollow spheres (a, b), the PANI-S composite (c, d), STEM image of PANI-S composite and the corresponding EDX elemental mappings of (f) carbon and (g) sulfur of the PANI-S. Scan bar: 1 μ m (a) and (c), 200nm (b), (d) and (e).

Fig.2a, Fig.2b and Fig. S2a show the TEM and SEM images of mono-disperse PANI hollow spheres, the diameter of them is in the range of 600-800 nm, and the thickness of shell is about 60nm. Both the large diameter and thin shell supply enough void space to hold more sulfur. The PANI hollow spheres maintains integrity after heat treatment with sulfur as shown in Fig.2c, Fig.2d and Fig.S2b, showing excellent stability. To analyze the distribution of the sulfur in the PANI hollow sphere based composite, elemental mapping and line scan analysis of sulfur in PANI-S composite are carried out. Fig.2e and Fig. 2f confirm the absence of sulfur particles in PANI-S composite, and the uniformly distribution of sulfur. Moreover, it attaches on both the inner and outer surface of PANI hollow spheres rather than diffusing into the internal void space.

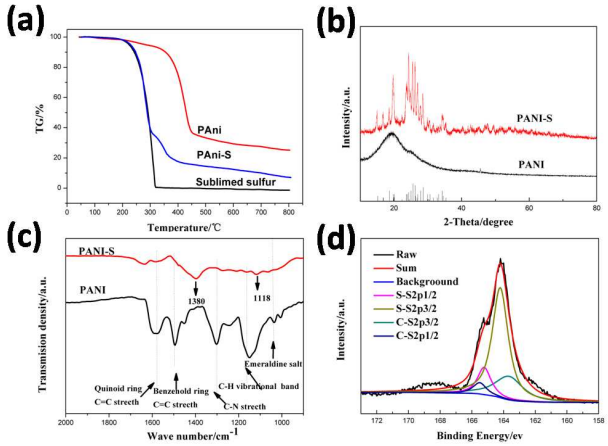

Fig.3 (a) TG curves of sublimed sulfur, PANI, and PANI-S composite, (b) the XRD patterns of sublimed S, hollow PANI sphere and PANI-S composite, (c) FTIR spectra of the PANI hollow sphere and PANI-S composite, (d) XPS spectrum of the PANI-S composite in S 2p region.

The content of sulfur in the PANI-S composite as determined by TG analysis is about 62wt%. As shown in Fig.3a. The weight loss before 320℃ is considered to be due to the evaporation of sulfur from the composites. Fig. 3b shows the XRD patterns of hollow PANI sphere and PANI-S composite. As seen, the PANI-S composite displays a very broad reflection peak, indicating an amorphous nature of the sulfur in the composite. During the co-heating process, the molten sulfur could be penetrated into the hollow PANI spheres with the help of capillary force and the strong absorbability of PANI to sulfur, finally forming a homogenous composite. FTIR measurement is further conducted on the PANI hollow spheres and PANI-S composites to characterize the presence of PANI and the structure change of the PANI matrix during the co-heating process. As shown in Fig. 3c, two characteristic peaks at 1568 and 1492 cm^{-1} are attributed to quinoid and benzenoid-ring vibrations, respectively, indicating the oxidation state of emeraldine base polyaniline. The bands in the 1200-1400 cm^{-1} range are the C-N stretching modes of an aromatic amine[33, 56]. However, there are significant differences in the FTIR spectrum of PANI-S from that of PANI sample. The C = C stretching vibration at 1497 cm^{-1} assigned to benzenoid rings shifts to lower wave numbers. The C-N stretching vibrational bands in the 1400 to 1200 cm^{-1} range also shift to lower wave numbers. The intensity of the C-H vibrational band in the vicinity of 1172 cm^{-1} is significantly weak, confirming the replacement of H atoms on aromatic rings by S atoms[54, 57]. Moreover, as shown in Fig.3d, the XPS spectrum of PANI-S composite in S 2p region also shows the generation of C-S bond during heat treatment[58]. These results show the fromation of stronger bonds between sulfur and PANI during the higher temperature treatment. These bonds are stronger than the H bond between PANI and S at low temperature[9]. Consequently, PANI-S composite could inhibit the

dissolution and migration of PS in the electrolyte effectively, indicating an enhanced cycling performance.

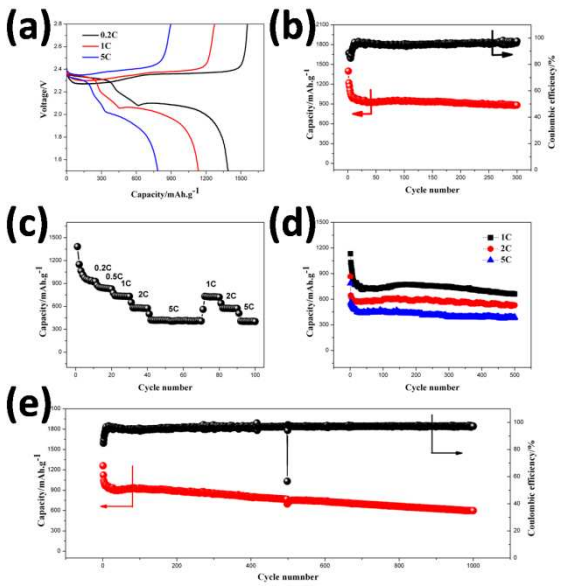

Fig. 4 (a) Initial discharge curves of PANI-S cathode at different rates, (b) the discharge capacity and efficiency coulombic cycling stability of PANI-S cathode at 0.2C, (c) rate performance of PANI-S cathode, (d) cycle life of the PANI-S cathode at 1C, 2C and 5C (e) prolonged cycle life of PANI-S cathode at 0.5C.

The discharge curves of the PANI-S composite at different rates are shown in Fig. 4a. Two voltage plateaus at about 2.38V and 2.08V are observed at 0.2C. The high voltage plateau corresponds to the reduction from elemental sulfur to PS. The low voltage plateau is attributed to the reduction of PS to Li_2S_2 and Li_2S[59-61]. Sulfur is dispersed uniformly on both the inner and outer surface of PANI hollow spheres because of the absorbing ability of PANI to S. Therefore, the active material has a sufficient contact with the liquid electrolyte, leading to higher utilization rate of sulfur. In addition to the electrochemically activity of PANI, the cells show improved initial discharge capacity, which is as high as 1392.7 $mAh.g^{-1}$ at 0.2C, 1133.4 $mAh.g^{-1}$ at 1C and 785.7 $mAh.g^{-1}$ at 5C respectively.

The cycling ability and the coulombic efficiency of PANI-S electrode at 0.2C are shown in Fig.4b. The serious capacity decay during the first 40 cycles is attributed to the dissolution of sulfur on the outer surface of PANI hollow sphere for the sample. After 40 cycles, the capacity at 300th cycle is as high as 802.5$mAh.g^{-1}$ with an average coulombic efficiency of 95.2%, which is 87.2% of the capacity at the 40th cycle. The S-C bond generated during higher temperature treatment, and sulfur trapped in the hollow holes of PANI hollow spheres, results in an excellent cycling stability during the following cycles.

Moreover, as seen in Fig.4c, the discharge capacity of PANI-S cathode returns to 731.8 $mAh.g^{-1}$ when the rate decreases from 5C to 1C. The excellent cycling performance and rate stability display a stable structure and good conductivity of the sulfur cathode. The long cycling performance of sulfur cathode at different rates is shown in Fig.4d. With capacity decay during the first several tens of cycles, the discharge capacities are still stable at 660 $mAh.g^{-1}$, 528 $mAh.g^{-1}$ and 381 $mAh.g^{-1}$ at 1C, 2C and 5C respectively after 500 charge/discharge cycles, which is about 90.4%, 89.6% and 87.3% of the capacity at the 50th cycle. Most importantly, The PANI-S cathode exhibits an excellent prolonged cycling stability, with its capacity always stabilizing around 767 $mAh.g^{-1}$ after 500 cycles at 0.5C, and its average coulombic efficiency approaches 97%, the high coulombic efficiency is attributed to the addition of $LiNO_3$ in the electrolyte[21] and the designed sulfur cathode. After 500 cycles, the battery is rested in ambient environment for 120h before running another 500 cycles. The rest process does not deteriorate the battery's performance, the discharge capacity returns to 752$mAh.g^{-1}$ after 10 cycles. The Li-S battery still shows fine working stability in the subsequent 500 cycles, and delivers a reversible capacity of 602 $mAh.g^{-1}$ after 1000 cycles, the capacity decay during 510~1000cycles is as small as 0.016% per cycle. And the charge/discharge profiles at different cycles are displayed in Fig. S3, as seen, the curves are similar to each other, indicating a reversible reaction during the charge/discharge process.

As seen in Fig.S4, the cycling performance of pure sulfur cathode in the same electrolyte is worse than that of PANI-S cathode. And the cycling performance of the PANI-S cathode in the electrolyte without $LiNO_3$ is still unsatisfactory. Therefore, the enhanced cycling performance is attributed to the designed sulfur cathode other than the modified electrolyte.

To get further insight into the electrochemical reaction process of the designed sulfur cathode, electrochemical impedance spectra (EIS) of the PANI-S at the fully charged state for different cycles are measured (Fig. S5). Generally, the impedance plots are composed of two semicircles corresponding to the charge transfer impedance and interfacial impedance respectively, and a sloping straight line in the low frequency domain corresponding to the Warburg impedance[56, 60]. Because of the shuttle effect during charge/discharge process, the redistribution of active material is unavoidable. This results in an inhomogeneous distribution of insulating sulfur on the surface of cathode and the corrosion of lithium anode, leading to the increased resistance during charge/discharge process[14]. The resistance (169Ω) especially the interfacial resistance (129Ω) before discharge is high owing to the insulating sulfur on the outer surface of the PANI hollow spheres. The impedance of the PANI-S sample decreases dramatically to the lowest value (119Ω) at the 5th cycle, indicating electrochemical activation and the dissolution of sulfur on the outer surface of PANI hollow sphere. Afterwards, the resistance value rises slightly to 193Ω at the 200th cycle. The resistance of the cell improves slowly during charge/discharge process, whereas the resistance increases a lot upon cycling with conventional Li-S cells[62]. This indicates the deposition and aggregation of sulfur on the surface of electrode are not serious and a stable cathode structure is obtained.

As obtained, PANI-S cathode shows greatly improved overall electrochemical performance. The calculation results (as seen in the Supplementary Information) show that the volume of Li_2S in PANI hollow spheres ($0.91cm^3.g^{-1}$) is smaller than the porous volume in PANI hollow spheres ($1.31cm^3.g^{-1}$), Therefore, it is reasonable to account for the existence of void space in the PANI-S nano-particles even after lithiation, which is beneficial to

gain a stable microstructure of the cathode. Correspondingly, the morphology of PANI-S cathode after 100 cycles was observed to understand the mechanism for the enhancement. As seen in Fig.S6, no obvious structural change of the cathode appears even after such a long cycling, indicating sufficient mechanical strength of the shell building the hollow PANI spheres. Furthermore, the elemental analysis results also show the maintenance of the uniform distribution of sulfur in PANI hollow sphere even after long cycling. The line scan analysis indicates little sulfur on the outer surface of PANI hollow sphere, while almost all of them deposit on the inner surface of PANI hollow spheres, unlike that of the PANI-S composite before cycling. Therefore, it is reasonable to explain the serious capacity fading during the first several tens of cycles by the loss of some sulfur weakly trapped on the outer surface of PANI hollow sphere. However, the major sulfur encapsulated inside the PANI hollow sphere is trapped by the cross-linked stereo PANI-S network and PANI shell, affording excellent cycling stability during the following cycles.

Above all, the excellent overall electrochemical behavior of the as prepared PANI-S cathode can be attributed to multiple, possibly synergistic factors that stem from its design. Firstly, the encapsulation of sulfur into the PANI hollow spheres, the adsorption effect between the hollow spheres and active material[63, 64], and the S-C bonds generated during heating treatment act as the bridge between the PANI and sulfur or PS. This inhibits the dissolution and migration of PS in the electrolyte, thus effectively enhancing the cycling stability and the coulombic efficiency of the electrode. Secondly, the shell of the hollow spheres with favorable dual conduction of Li^+ and electron is beneficial to the enhancement of rate capability of the sulfur cathode. Thirdly, the designed void space in PANI hollow spheres supply sufficient space to buffer the large volume expansion of sulfur during the charge/discharge process, resulting in a stable structure of the cathode, and therefore long stability of lithium sulfur battery.

Conclusions

PANI hollow sphere has been synthesized using sulfonated polystyrene spheres as the template. With a vapor phase infusion method, the composite of sulfur and PANI hollow sphere is further fabricated. Li-S battery with the as prepared cathode displays an excellent overall electrochemical behaviors, especially for the high columbic efficiencies, outstanding rate stability and cycling performance. Three factors are attributed to the excellent overall performance. Firstly, the dissolution and migration of PS in the electrolyte is inhibited by PANI shell and chemical bond formed during heating treatment process. Secondly, the dual conduction of electron and Li^+ of PANI thin shell improves the conductivity of the cathode. Thirdly, the volumetric expansion of sulfur cathode during lithiation is suppressed due to the presence of sufficient internal void space in PANI-S composite.

Acknowledgements

This work was financially supported by NSFC Project No.51373195, NO.51372262 and No.51272267; research projects from the Science and Technology Commission of Shanghai Municipality No. 08DZ2210900.

We thank Prof. B. V. R. Chowdari (Department of Physics, National University of Singapore) for helpful discussions.

Notes and references

[a] *Shanghai Institute of Ceramics, Chinese Academy of Sciences, Shanghai 200050, P. R. China Fax: +86-21-52413903; Tel: +86-21-52411704; E-mail: zywen@mail.sic.ac.cn*

[b] *Department of Materials Science and Engineering, University of Science and Technology of China, Hefei 230026, P. R. China E-mail: cchchen@ustc.edu.cn*

† Electronic Supplementary Information (ESI) available: [details of any supplementary information available should be included here]. See DOI: 10.1039/b000000x/

1. S. A. F. Peter G. Bruce, Laurence J. Hardwick and Jean-Marie Tarascon, *Nat Mater*, 2012, **11**. 19-29
2. S. E. A. L. F. NAZAR, *Accounts Chem Res*, 2012, 46(5), 1135-1143.
3. Y. Yang, G. Zheng and Y. Cui, *Chem Soc Rev*, 2013, **42**, 3018-3032.
4. B. Dunn, H. Kamath, J. M. Tarascon, *Science*, 2011, **334(6058)**, 928-935.
5. H. Kim, H. D. Lim, J. Kim and K. Kang, *Journal of Materials Chemistry A*, 2013, **2**, 32-47.
6. G. Zheng, Q. Zhang, J. J. Cha, Y. Yang, W. Li, Z. W. Seh and Y. Cui, *Nano Lett*, 2013, **13**, 1265-1270.
7. G. Zheng, Y. Yang, J. J. Cha, S. S. Hong and Y. Cui, *Nano Lett*, 2011, **11**, 4462-4467.
8. Y. F. ARUMUGAM MANTHIRAM, Y. S. SU, *Accounts Chem Res*, 2012, 46(5), 1125-1134.
9. S. S. Zhang, *J Power Sources*, 2013, **231**, 153-162.
10. J. L. Wang, J. Yang, C. R. Wan, K. Du, J. Y. Xie and N. X. Xu, *Adv Funct Mater*, 2003, **13**, 487-492.
11. S. E. Cheon, K. S. Ko, J. H. Cho, S. W. Kim, E. Y. Chin and H. T. Kim, *Journal of the Electrochemical Society*, 2003, **150**, A796-A799.
12. D. Wang, Q. Zeng, G. Zhou, L. Yin, F. Li, H.-M. h. Cheng, I. Gentle, G. Q. Lu, *Journal of Materials Chemistry A*, 2013, **1**, 9383-9394.
13. Z. Wei Seh, W. Li, J. J. Cha, G. Zheng, Y. Yang, M. T. McDowell, P. C. Hsu and Y. Cui, *Nature Communications*, 2013, **4**, 1331-1336.
14. J. Zheng, M. Gu, C. Wang, P. Zuo, P. K. Koech, J. G. Zhang, J. Liu and J. Xiao, *Journal of the Electrochemical Society*, 2013, **160**, A1992-A1996.
15. N. A. Cañas, S. Wolf, N. Wagner and K. A. Friedrich, J Power Sources, 2013, 226, 313-319
16. S. S. Zhang, *Electrochem Commun*, 2013, **31**, 10-12.
17. R. Demir-Cakan, M. Morcrette, Gangulibabu, A. Guéguen, R. Dedryvère and J.-M. Tarascon, *Energ Environ Sci*, 2013, **6**, 176-182.
18. L. Suo, Y.-S. Hu, H. Li, M. Armand and L. Chen, *Nature Communications*, 2013, **4**, 1481-1489.
19. J. W. Park, K. Yamauchi, E. Takashima, N. Tachikawa, K. Ueno, K. Dokko and M. Watanabe, *The Journal of Physical Chemistry C*, 2013, **117**, 4431-4440.
20. D.-J. Lee, M. Agostini, J.-W. Park, Y.-K. Sun, J. Hassoun and B. Scrosati, *Chemsuschem*, 2013, 6, 2245-2248.

21. X. Liang, Z. Y. Wen. Y. Liu, M. F. Wu, J. Jin, H. Zhang, X. W. Wu, *J Power Sources*, 2011, **196**. 9839-9843.
22. L. Ji, M. Rao, S. Aloni, L. Wang, E. J. Cairns and Y. Zhang, *Energ Environ Sci*, 2011, **4**, 5053-5059.
23. K. T. Lee, R. Black, T. Yim, X. Ji and L. F. Nazar, *Adv Energy Mater*, 2012, **2**, 1238-1245.
24. N. Jayaprakash, J. Shen, S. S. Moganty, A. Corona and L. A. Archer, *Angewandte Chemie International Edition*, 2011, **50**, 5904-5908.
25. K. Zhang, Q. Zhao, Z. Tao and J. Chen, *Nano Res*, 2012, **6**, 38-46.
26. T. Lin, Y. Tang, Y. Wang, H. Bi, Z. Liu, F. Q. Huang, X. Xie and M. Jiang, *Energ Environ Sci*, 2013, **6**, 1283-1290.
27. Z. Zeng, X. Gui, Z. Lin, L. Zhang, Y. Jia, A. Cao, Y. Zhu, R. Xiang, T. Wu and Z. Tang, *Adv Mater*, 2013, **25**, 1185-1191.
28. R. Elazari, G. Salitra, A. Garsuch, A. Panchenko and D. Aurbach, *Adv Mater*, 2011, **23**, 5641-5644.
29. B. Zhang, X. Qin, G. R. Li and X. P. Gao, *Energ Environ Sci*, 2010, **3**, 1531-1537.
30. G. C. Li, J. J. Hu, G. R. Li, S. H. Ye and X. P. Gao, *J Power Sources*, 2013, **240**, 598-605.
31. L. X. Miao, W. K. Wang, A. B. Wang, K. G. Yuan and Y. S. Yang, *Journal of Materials Chemistry A*, 2013,**1(38)**, 11659-11664.
32. L. Yin, J. Wang, F. Lin, J. Yang and Y. Nuli, *Energ Environ Sci*, 2012, **5**, 6966-1672.
33. M. Wang, W. Wang, A. Wang, K. Yuan, L. Miao, X. Zhang, Y. Huang, Z. Yu and J. Qiu, *Chem Commun*, 2013, **49(87)**, 10263-10265.
34. H. Chen, W. Dong, J. Ge, C. Wang, X. Wu, W. Lu and L. Chen, *Scientific Reports*, 2013, **3**.
35. M. J. Lacey, F. Jeschull, k. Edström and D. Brandell, *Chem Commun*, 2013, **49(76)**, 8531-8533.
36. F. Wu, J. Z. Chen, R. J. Chen, S. X. Wu, L. Li, S. Chen and T. Zhao, *J Phys Chem C*, 2011, **115**, 6057-6063.
37. Y. Fu and A. Manthiram, *Rsc Adv*, 2012, **2**, 5927-5929.
38. Y. Fu, Y. S. Su and A. Manthiram, *Angewandte Chemie International Edition*, 2013, **52**, 6930-6935.
39. Y. Fu, Y. S. Su and A. Manthiram, *Adv Energy Mater*, 2014, **4(1)**, 1-5.
40. S. H. Choi and Y. C. Kang, *Small*, 2013.
41. B. R. S. Lemos, I. F. Teixeira, B. F. Machado, M. R. A. Alves, J. P. de Mesquita, R. R. Ribeiro, R. R. Bacsa, P. Serp and R. M. Lago, *Journal of Materials Chemistry A*, 2013, **1**, 9491-9497.
42. Z. Jin, K. Xie, X. Hong, Z. Hu and X. Liu, *J Power Sources*, 2012, **218**, 163-167.
43. J. Q. Huang, Q. Zhang, H.-J. Peng, X. Y. Liu, W. Z. Qian and F. Wei, *Energ Environ Sci*, 2014, **7**, 347-353.
44. M. Hagen, S. Dorfler, H. Althues, J. Tubke, M. J. Hoffmann, S. Kaskel and K. Pinkwart, *J Power Sources*, 2012, **213**, 239-248.
45. S. H. Chung, A. Manthiram, *Journal of Materials Chemistry A*, 2013, **1**, 9590-9596.
46. C. Zu, Y. Fu and A. Manthiram, *Journal of Materials Chemistry A*, 2013, **1**, 10362-10367.
47. B. Duan, W. Wang, H. Zhao, A. Wang, M. Wang, K. Yuan, Z. Yu and Y. Yang, *ECS Electrochemistry Letters*, 2013, **2**, A47-A51.
48. Y. M. Lee, N.-S. Choi, J. H. Park and J.-K. Park, *J Power Sources*, 2003, **119-121**, 964-972.
49. W. Li, G. Zheng, Y. Yang, Z. W. Seh, N. Liu and Y. Cui, *Proceedings of the National Academy of Sciences*, 2013, 110(18), 7148-7153.
50. W. Li, Q. Zhang, G. Zheng, Z. W. Seh, H. Yao and Y. Cui, *Nano Lett*, 2013, **13**, 5534-5540.
51. J. X. Huang, S. Virji, B. H. Weiller and R. B. Kaner, *J Am Chem Soc*, 2003, **125**, 314-315.
52. Q. Wu, Z. Wang and G. Xue, *Adv Funct Mater*, 2007, **17**, 1784-1789.
53. S. Virji, J. X. Huang, R. B. Kaner and B. H. Weiller, *Nano Lett*, 2004, **4**, 491-496.
54. W. Zhou, Y. Yu, H. Chen, F. J. DiSalvo and H. D. Abruña, *J Am Chem Soc*, 2013, **135**, 1636-1643.
55. W. Zhou, Y. Yu, H. Chen, F. J. DiSalvo and H. D. Abruña, *J Am Chem Soc*, 2013, **135**, 16736-16743.
56. G.-C. Li, G.-R. Li, S.-H. Ye and X.-P. Gao, *Adv Energy Mater*, 2012, **2**, 1238-1245.
57. L. Xiao, Y. Cao, J. Xiao, B. Schwenzer, M. H. Engelhard, L. V. Saraf, Z. Nie, G. J. Exarhos and J. Liu, *Adv Mater*, 2012, **24**, 1176-1181.
58. S. Xin, L. Gu, N. H. Zhao, Y. X. Yin, L. J. Zhou, Y. G. Guo and L. J. Wan, *J Am Chem Soc*, 2012, **134**, 18510-18513.
59. M. Xiao, M. Huang, S. Zeng, D. Han, S. Wang, L. Sun and Y. Meng, *Rsc Adv*, 2013, **3**, 4914-4916.
60. Y. Fu, Y.-S. Su and A. Manthiram, *Acs Appl Mater Inter*, 2012, **4**, 6046-6052.
61. Z. W. Seh, H. Wang, P.-C. Hsu, Q. Zhang, W. Li, G. Zheng, H. b. Yao and Y. Cui, *Energ Environ Sci*, 2014.
62. Y. S. Su and A. Manthiram, *Electrochim Acta*, 2012, **77**, 272-278.
63. J. X. Song, T. Xu, M. L. Gordin , P. Y. Zhu , D. P. Lv, Y. B. Jiang, Y. S. R. Chen, Y. H. Duan, and D. H. Wang, *Adv. Funct. Mater.* **2014**, *24*, 1243–1250.
64. T. Xu, J. X. Song, M. L. Gordin, H. Sohn, Z. X. Yu, S. R. Chen, and D. H. Wang, *ACS Appl. Mater. Interfaces* 2013, 5, 11355−11362.